PNAS RESEARCH ARTICLE | ENVIRONMENTAL SCIENCES OPEN ACCESS

Postglacial ecosystem development of a hydrothermal landscape in Yellowstone National Park

Cathy Whitlock[a,b,1], Christopher M. Schiller[c], Steven W. Hostetler[d], Shaul Hurwitz[e], Mio Alt[a,b], Sabrina R. Brown[f], Lauren N. Harrison[g], Jay R. Alder[h], Kailey Busch[a,b], Jake Shelly[a,b], and David B. McWethy[a,b]

Affiliations are included on p. 10.

Contributed by Cathy Whitlock; received April 29, 2026; accepted July 15, 2026; reviewed by Sherilyn C. Fritz and Jennifer Pierce

The Yellowstone geo-ecosystem has been the subject of much research, but the ecological history of the Yellowstone Plateau volcanic field and its iconic geyser basins is less known. In this investigation, paleoenvironmental analyses of sediment cores from lakes in Lower Geyser Basin were compared with regional records and paleoclimate model simulations to reconstruct the vegetation, wildfire, limnology, hydrothermal dynamics, and climate drivers since deglaciation, 15,000 to 14,000 years ago. Pollen data from Lower Geyser Basin lakes reveal the strong influence of infertile rhyolitic soils on vegetation history: an initial late-glacial steppe was replaced by lodgepole pine forest from 12.8 to 11.0 ka, with little change in forest composition or cover thereafter despite changing climate. This stability contrasts with the more dynamic vegetation response on nonrhyolite substrates in the Yellowstone region where nutrient and moisture availability is greater. Highest wildfire activity and low lake nutrient levels in Lower Geyser Basin occurred from 12 to 4 ka, when summers were substantially warmer and drier and fire-inducing vapor pressure deficits were 29 to 56% higher. The hydrothermal history, inferred from sedimentary arsenic and cesium abundances, was spatially and temporally variable but lake-forming hydrothermal events align with periods of abundant moisture. Thus, long-term changes in wildfire, limnology, and, to some extent, hydrothermal activity were governed by insolation-driven climate variations, whereas the vegetation response was muted and constrained by geologic processes. These findings suggest that warmer, drier conditions in the future could result in less hydrothermal activity yet little change in forest cover across the Yellowstone Plateau volcanic field despite more wildfires.

Yellowstone | geyser basin | Holocene history | paleoclimate | pollen

Significance

Yellowstone's thermal areas are dynamic geo-ecosystems shaped by geological, climatic, and ecological processes. Analysis of lake-sediment cores from Lower Geyser Basin suggests that postglacial lakes formed in depressions created by climate-influenced hydrothermal explosions; these lakes have had hydrothermal input since their inception. Warmer and drier conditions than present from 12,000 to 4,000 years ago led to shallow nutrient-limited lake conditions and high wildfire activity. Despite past variations in climate, forests within the geyser basins and surrounding volcanic region have changed little due to edaphic constraints that favor lodgepole pine over other conifers. The geo-ecological history of the geyser basin and surrounding area suggests that future warming might lead to less hydrothermal activity and more wildfires but little change in vegetation.

The Yellowstone Plateau volcanic field covers an area of ~17,000 km^2 of Wyoming, Idaho, and Montana, with most volcanic and hydrothermal activity located within Yellowstone National Park (Fig. 1). The volcanic field has been profoundly shaped by three cataclysmic volcanic eruptions in the past 2.1 Ma that emplaced voluminous rhyolite tuffs (1). Eruption of the Lava Creek Tuff at 631 ± 4.3 ka (1, 2) formed the Yellowstone Caldera (85 km by 45 km), which is now filled with >360 km^3 of rhyolite lava flows with the most recent from an eruption ~70 ka ago (1, 3). The Yellowstone Caldera and its surroundings currently host the largest and most diverse hydrothermal system in the continental crust, with more than 10,000 thermal features including geysers, hot springs, and fumaroles (4, 5).

Hydrothermal activity in the volcanic field is modulated by changes in meteoric water supply and subsurface permeability. Geysers are among the most unique features of Yellowstone's hydrothermal system, and changes in their activity have resulted from large earthquakes (12) and shifts in climate over time (13–15). Groundwater is largely derived from winter snowmelt and heated along the subsurface flowpath by a magmatic source. Snowpack and thus groundwater recharge rates vary at timescales ranging from seasons to millennia (16), which in turn affects hydrothermal activity (4, 17). For example, a megadrought associated with sustained low snowpack during the Medieval Climate Anomaly (900–1300 CE) reduced water supply, leading to the cessation of eruptions of Old Faithful Geyser from the mid-13th to the mid-14th century, and periods of severe drought in the 15th to 17th centuries halted eruptions of Steamboat Geyser (13, 14).

In most of the western United States, forest composition is largely controlled by physical gradients (e.g., climate, elevation, aspect, soil) that influence nutrient availability and growing-season conditions (e.g., length, temperature, and available moisture). Subalpine forests on nonrhyolite substrates in the Yellowstone region, for example, are dominated by Engelmann spruce (*Picea engelmannii*), subalpine fir (*Abies lasiocarpa*), and white pines

Reviewers: S.C.F., University of Nebraska-Lincoln; and J.P., Boise State University Department of Geosciences.

Competing interest statement: Reviewer S.C.F. and co-authors of this paper collaborated on a multi-investigator paper that was published online in 2022 on work that was completed in 2021; we have not collaborated since then.

[1]To whom correspondence may be addressed. Email: whitlock@montana.edu.

This article contains supporting information online at https://www.pnas.org/lookup/suppl/doi:10.1073/pnas.2613422123/-/DCSupplemental.

Published August 17, 2026.

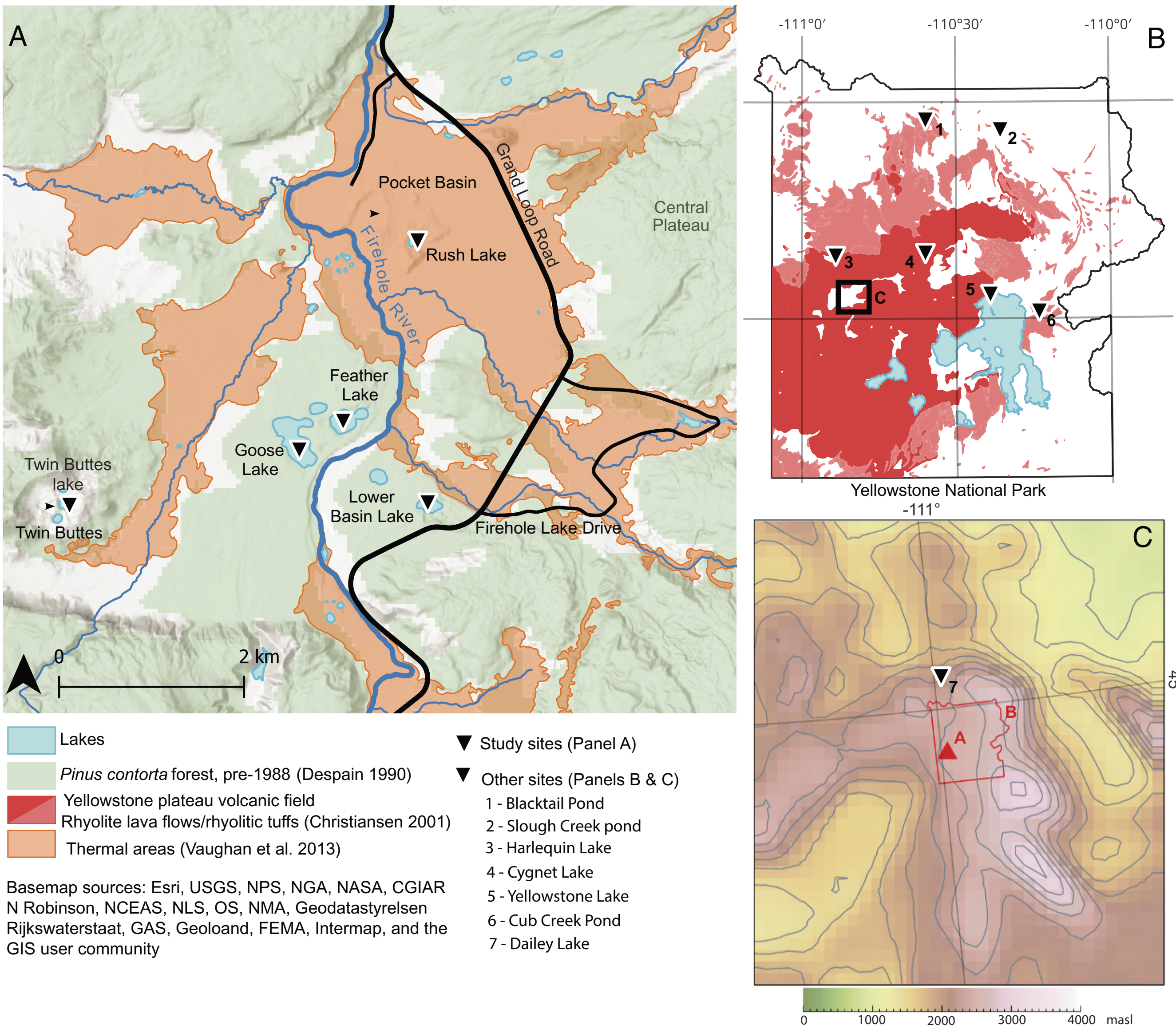

Fig. 1. Maps showing locations discussed in text. (*A*) Location of study sites in Lower Geyser Basin with respect to forest and thermal areas (6, 7). (*B*) Location of Lower Geyser Basin and the Yellowstone Plateau volcanic field within Yellowstone National Park (8); numbers identify other sites in the regional comparison (9–11). (*C*) Topography of the Yellowstone region on the Lambert Conformal Conic projection used in the RegCM5 climate model; also shown are the locations of panels *A* (red triangle) and *B* (red Yellowstone National Park), as well as Dailey Lake (site 7) (11).

(*Pinus albicaulis* and *Pinus flexilis*); lodgepole pine (*Pinus contorta*) in these settings acts as a fire-adapted early successional species (6). In contrast, subalpine forests on Yellowstone's rhyolite lava flows and glacial deposits within the geyser basins are composed of lodgepole pine through all seral stages, as a result of the limited nutrients (low concentrations of Ca, Mg) and low water-holding capacity of coarse-textured rhyolite-derived soils (6).

Studies elsewhere in North America have shown that, in some settings, the nutrient and moisture availability of soils can strongly influence the response of plant communities to the effects of long-term climate change (e.g., refs. 18 and 19). The ecological history on rhyolite substrates within the Yellowstone Plateau volcanic field is known from only three lake-sediment records: a late-glacial-Holocene sequence from the Central Plateau region (9), a Holocene record from Yellowstone Lake (10), and a Holocene record from Lower Geyser Basin (20) (Fig. 1). With so few records and limited paleoclimate information, knowledge of centennial-to-millennial geologic and climatic influences on ecosystem evolution within the volcanic field, particularly the geyser basins, is limited.

To broaden understanding of postglacial geo-ecosystem dynamics in the Yellowstone region, we reconstruct the vegetation, wildfire, limnological, and hydrothermal history of the largest thermal area, Lower Geyser Basin (Fig. 1*A*). Sediment-core records from small lakes are evaluated against i) regional climate model simulations that portray changes in temperature, precipitation, and other climate variables; ii) independent studies documenting past hydrothermal activity; and iii) paleoenvironmental proxies from the broader Yellowstone region. We hypothesize that Lower Geyser Basin has been shaped by changes in climate over short (interannual to decadal) and long (centennial to millennial) time scales but that the vegetation response has been constrained by the underlying geology. Our results provide insights into the environmental history of an active geyser basin as well as its sensitivity to past and future climate change. This information provides guidance for tracking changes in hydrothermal activity and ecological change and for managing the unique natural resources of Yellowstone National Park.

Lower Geyser Basin

Lower Geyser Basin covers an area of ~28.5 km^2 at an average elevation of 2,240 m above sea level. The generally flat basin is covered by glacial till with varying degrees of hydrothermal alteration, silica sinter deposits, hydrothermal explosion craters, and a few exposures of Upper Basin Member rhyolite flows (~580 to ~255 ka). It is surrounded by the Central Plateau Member (~160 to ~70 ka) of the Plateau Rhyolite (21). The basin hosts extensive hydrothermal activity, including active and dormant geysers, mostly alkaline hot springs, mudpots, and fumaroles. During the Pinedale glaciation (Marine Isotope Stage 2), ~22 to ~14 ka, the Yellowstone region was covered by a complex glacial system that at its peak was >1 km thick (22). Based on the timing of glacial retreat mapped in other parts of Yellowstone, Lower Geyser Basin ice recession occurred between 14 to 15 ka (22).

Within Lower Geyser Basin, high soil temperatures create unique thermal grassland communities (30 to 50 °C) and barren sinter flats (>50 °C) (23). Lodgepole pine forest grows on unheated ground (<8 °C) and rhyolitic soils, and sagebrush (*Artemisia tridentata*) steppe is present in areas of clay-rich glacial deposits (6, 24). Mean annual air temperature between 1991 and 2020 within the geyser basin was 1.4 °C, ranging from −9.9 °C in December to 14.3 °C in July (25). Precipitation in the Yellowstone region is strongly influenced by topography, with 85% of the average annual received in October through May from Pacific storm systems tracking up the Snake River Plain (26). In contrast, precipitation in June through September is mainly delivered from isolated convective storms because the seasonal intensification of the northeastern Pacific subtropical high-pressure system suppresses Pacific moisture ["summer-dry" sensu Whitlock and Bartlein (27)]. Peak wildfire season is from July to September (28).

The five study lakes in Lower Geyser Basin (Fig. 1*A* and Table 1) lie in topographic depressions in glacial deposits, freeze during winter months, and have no or limited surface inlets or outlets. Hydrothermal explosion craters have been described at Twin Buttes, Pocket Basin, and Rush Lake (29, 30), but the depressions that contain Goose, Feather, Rush, and Lower Basin lakes have not been formally classified as hydrothermal explosion craters. Goose, Feather, and Lower Basin lakes are identified as mesotrophic (moderate nutrient concentrations and level of primary productivity) (31). The water chemistry of Goose and Lower Basin lakes is similar but more dilute than the alkaline hot springs in Lower Geyser Basin, suggesting the lakes receive a mixture of hydrothermal input and meteoric water from melting snow and ice. In Feather and Lower Basin lakes, concentrations of major solutes (chloride, sodium, alkalinity) and arsenic (As) (0.74 to 0.95 mg/L) are approximately half of the concentration in the surrounding hot springs (32). At larger Goose Lake, the fraction of thermal water is significantly smaller than at Feather or Lower Basin lakes. At Rush Lake, low concentrations of chloride and high concentrations of sulfate (SO_4) suggest a fraction derived from acid-sulfate waters.

Research Approach

Sediment cores were collected in 2023–2024 from Rush, Feather, Lower Basin, and Twin Buttes lakes (Table 1 and *Materials and Methods*). The Goose Lake core was collected in 2018 with results described in Schiller et al. (20). Lithologic terminology followed Zahajská et al. (33) and Schnurrenberger et al. (34). A chronology for each lake record was established from calibrated radiocarbon dates on charcoal and terrestrial plant macrofossils and from tephrochronology. Age-depth models were developed with the IntCal20 calibration curve (35) using Bacon software (36) and reported in ka (kiloannum before 1950 CE) (*SI Appendix*, Fig. S1 and Table S1). Identification of the Mazama ash [7.584 to 7.682 ka; (37)] and Glacier Peak ash [13.41 to 13.71 ka; (38)] in the sediment cores, based on single-grain microbe analyses, helped constrain age determinations. The paucity of terrestrial organic material in the cores and presence of erroneously old-biased radiocarbon dates [from the introduction of ancient carbon in thermal waters (39)] meant that the age-depth models were based heavily on tephrochronology, lithostratigraphy, and glacial history.

Different proxies in Lower Geyser Basin are controlled by hydrothermal processes and climate to varying degrees. The concentration of arsenic (As) and cesium (Cs), which are elevated in Yellowstone's thermal waters (32), was measured in the sediment by scanning X-ray fluorescence (XRF). Because XRF output is reported in counts per second (cps) (*SI Appendix*), the results were standardized and presented as relative concentrations. High As and Cs concentrations are considered evidence of hydrothermal enrichment, but temporal variations in their abundance may be influenced by other processes. For example, arsenic concentrations in lake sediments are affected by subaqueous redox, precipitation of As-rich secondary minerals, and adsorption and coprecipitation of As on iron minerals and sedimentary organic matter (40).

Table 1. Lower Geyser Basin site information

Site	Location	Elevation (masl)*	Surrounding vegetation	Surface area (m^2)	Maximum water depth (m)	Composite core length (m)	Analyses*	Inferred maximum age (ka)
Rush Lake	44.56159°N, 110.82654°W	2,200	Thermal grassland, *P. contorta* forest	700	0.7	7.10	XRF, $\delta^{13}C$, pollen, charcoal, diatoms	~14.2
Feather Lake	44.54401°N, 110.83641°W	2,197	*P. contorta* forest, *Artemisia* steppe	68,100	8.63	3.67	XRF, $\delta^{13}C$, pollen, 4 diatom samples	~8.8
Goose Lake†	44.54135°N, 110.84237°W	2,200	*P. contorta* forest, *Artemisia* steppe	148,000	8.86	8.09	XRF, $\delta^{13}C$, pollen, charcoal, diatoms	>10.3
Lower Basin Lake	44.53610°N, 110.82466°W	2,206	*P. contorta* forest, nearby thermal grassland	30,000	4.65	3.01	XRF, $\delta^{13}C$	<7.6
Twin Buttes lake	44.53600°N, 110.87363°W	2,276	*Artemisia* steppe; *P. contorta* forest	10,000	3.43	5.90	XRF, 3 pollen samples	>12.7

*masl is meters above sea level; XRF refers to scanning X-ray fluorescence; $\delta^{13}C$ is sediment derived.
†Schiller et al. (20).

Cesium can be precipitated to form a secondary zeolite mineral, analcime (41). We posit that variations in As and Cs concentration in the cores relate to different levels of hydrothermal input but acknowledge that additional research is needed to understand this relationship. In addition to As and Cs, stable carbon isotope ($\delta^{13}C$) analysis of bulk sediments was undertaken to determine whether the carbon source was organic terrestrial or hydrothermal.

The vegetation and wildfire history of Lower Geyser Basin was developed from pollen and charcoal data at Rush, Goose, Feather, and Twin Buttes lakes. Changes in pollen assemblages document past vegetation responses to variations in climate, wildfire, and other disturbances (*Materials and Methods*). Changes in the accumulation rates of macroscopic charcoal particles >125 μm in size (particles $cm^{-2}\ y^{-1}$) record shifts in local, stand-replacing wildfires (42, 43). Long-term variations in charcoal accumulation rates (CHAR) indicate millennial-scale changes in biomass burning shaped by fuels and climate. In addition to the Lower Geyser Basin sites, data from Harlequin Lake (charcoal) and Cygnet Lake (pollen, charcoal) in nonthermal areas within the Yellowstone Caldera and pollen records outside the Yellowstone Plateau volcanic field were considered in the regional analysis (Fig. 1 *B* and *C*).

Limnologic interpretations are based on diatom analysis of the Rush, Goose, and to a limited extent, Feather and Lower Basin lake cores. Changes in diatom composition reflect shifts in water chemistry and temperature that are controlled by hydrothermal inputs, lake level, and climate.

To assess the importance of past climate change in driving ecological dynamics and variations in hydrothermal activity, the RegCM5 regional climate model was used to simulate changes in annual temperature, annual precipitation, annual and summer effective moisture (precipitation minus evaporation; P–E), and snow water equivalent (SWE; a standardized measure of liquid water contained in the snowpack on April 1) (44) (*Materials and Methods*). These variables influence hydrology, vegetation distribution and composition, soil moisture and nutrient availability, and groundwater recharge. Fire-related metrics, such as solar radiation (insolation), July–September air temperature, and vapor pressure deficit (VPD), were examined to estimate trends in wildfire activity (45, 46). Model output is presented for the Yellowstone region with a focused examination of Lower Geyser Basin and expressed as 12, 9, 6, and 3 ka anomalies from the pre-Industrial present (0 ka).

Results

Lithologic and Geochemical Records. The stratigraphic records are discussed from oldest to youngest. In referencing the lithology and geochemistry, median calibrated ages are rounded to the nearest 100 years with 95% CI. Table 1 provides site information; core and geochemical stratigraphy is presented in *SI Appendix*, Fig. S2.

The Rush Lake core has an extrapolated basal age of 14.2 ka (95% CI 14.5 to 13.8 ka). The basal sediments (7.01 to 3.89 m depth) chiefly consist of interlaminated to interbedded clay, obsidian-rich sand, and gravel. An overlying diatom ooze from 3.89 m depth (12.6 ka, 95% CI 13.0 to 12.2 ka) to the surface registers productive limnic conditions. Glacier Peak and Mazama ashes were identified at 5.73 m and 2.30 m depth. A thick gravel unit at 6.41 to 6.34 m depth (13.9 ka, 95% CI 14.2 to 13.3 ka) shares characteristics, such as large grain size and hydrothermally altered clasts, with hydrothermal explosion deposits studied elsewhere in the region (47). These deposits may be ejecta from a hydrothermal explosion at nearby (~350 m distance) Pocket Basin, dated at 13.44 ± 1.06 ka (48).

The Rush Lake basin apparently formed from a hydrothermal explosion (29, 30) during deglaciation and prior to the Pocket Basin explosion and deposition of Glacier Peak ash [95% CI 13.71 to 13.41 ka; (38)]. Arsenic and Cs concentrations in sediments between 3.95 m depth and the top of the core are relatively low, which is consistent with the lake being a vapor-dominated, acid-sulfate system (49). The $\delta^{13}C_{sediment}$ values at 5.75 m, 4.80 m, 3.20 m, 2.29 m, 1.60 m, and 0.00 m depth range from −28.0 to −18.7‰ VPDB, suggesting a mixture of carbon from terrestrial organic sources and dissolved inorganic carbon from thermal waters (50, 51).

Twin Buttes is a thermal kame with at least three nested hydrothermal explosion craters on top that date to 13.56 ka (95% CI 11.28 to 15.84 ka) (48). A large landslide deposit contains several small ponds near the summit. Twin Buttes lake, an informal name for the largest, easternmost pond, formed before 12.7 ka, based on radiocarbon dates near the core base at 5.90 m depth (*SI Appendix*, Table S1). Late-glacial inorganic silt and clay transitioned to diatom ooze at 4.85 m depth (11.1 ka, 95% CI 11.2 to 10.8 ka) and peaty sapropel at 3.57 m depth. Neither Glacier Peak nor Mazama ashes were recovered in the core. Three pollen samples (5.49 to 5.53 cm depth) from the basal clay are dominated by nonarboreal pollen (*Artemisia*, Poaceae), corroborating a late-glacial age assignment for the lake (*SI Appendix*, Table S2).

At Goose Lake, the deepest recovered core sample at 8.09 m depth (10.3 ka, 95% CI 10.6 to 10.0 ka) consists of laminated diatom ooze, but the lake is likely older (20). Diatom ooze extends from 8.09 to 1.78 m depth (3.8 ka, 95% CI 4.3 to 3.5 ka). A thin layer from 6.29 to 6.28 m depth (7.9 ka, 95% 8.1 to 7.8 ka) consists of fluorite-rich mud (81.1 wt % fluorite) of hydrothermal provenance. From 1.78 to 0.20 m depth, sediments consist of thinly bedded diatom ooze and sapropel, and the upper 20 cm is massive diatomaceous sapropel. Relative As concentrations in Goose Lake sediments are initially high, indicating significant hydrothermal input in the early Holocene, and decline sharply at 1.78 m depth (3.8 ka, 94% 4.3 to 3.5 ka). A shift in average $\delta^{13}C_{sediment}$ values from −12.47‰ VPDB below 1.78 m depth to −23.05‰ VPDB above that depth also suggests a shift from hydrothermal to terrestrial carbon sources in the late Holocene (20). Relative Cs concentrations show no clear trend.

Feather Lake lies in a closed depression adjacent to Goose Lake. Basal sediments consist of laminated and massive clay layers (base 3.67 m depth; 8.8 ka, 95% CI 9.5 to 8.3 ka), which grade upward at 2.26 m depth (6.8 ka, 95% CI 7.2 to 6.4 ka) to interbedded layers of diatom ooze, sapropel, and sapropelic silt. Relative concentrations of As and Cs at Feather Lake increase from 2.00 to 1.40 m depth (5.5 to 3.7 ka, 95% CI 5.9 to 3.4 ka) and from 1.25 to 0 m depth (3.3 ka to present, 95% CI 3.7 to present), indicating more hydrothermal input in the upper sediments. The $\delta^{13}C_{sediment}$ values in samples at 3.60, 3.065, 2.40, 1.20, and 0.005 m depths range from −25.6 to −20.5‰ VPDB, consistent with a terrestrial organic source. Relative As concentrations at Feather Lake were low before 5.5 ka and elevated from 3.3 ka to present.

Lower Basin Lake lies in a forested depression adjacent to an active hydrothermal area and thermal grasslands along White Creek, a tributary of the Firehole River (Fig. 1*A*). Lack of suitable organic material for dating makes it difficult to determine the age of origin but based on its short sedimentary record that lacks Mazama ash, we posit a late-Holocene age. Sediment cores contain basal obsidian-rich gravel deposits (3.01 to 2.95 m depth) that suggest a hydrothermal origin. These deposits are overlain by peat (2.95 to 0.95 m depth) that is overlain by diatom ooze above 0.95 m depth. Relative As and Cs concentrations are depleted in the peat units and enriched in the diatom ooze, with a general increase up core, especially above 0.90 m depth. The $\delta^{13}C_{sediment}$ values in samples from 2.24 and 0.40 m depth are −26.8 and −17.0‰ VPDB, suggesting terrestrial organic and hydrothermal sources.

In sum, Rush and Twin Buttes lakes lie within mapped hydrothermal explosion craters (21). Feather, Lower Basin, and Goose lakes are in isolated depressions with elevated rims, suggesting their inception following hydrothermal explosions. Rush and Twin Buttes lakes developed in the late-glacial period, Goose and Feather lakes formed during the late-glacial-to-early Holocene transition, and Lower Basin Lake likely formed in the late Holocene. Elevated and sustained relative concentrations of sedimentary As and Cs in all lakes indicate persistent hydrothermal input since their origin.

Vegetation, Wildfire, and Limnobiotic Records. The paleoenvironmental records are organized into four periods: late-glacial (ca. 15 to 11.5 ka), early Holocene (ca. 11.5 to 8 ka), middle Holocene (ca. 8 to 4 ka), and late Holocene (ca. 4 ka–present). Because the chronology for and comparison of pollen, charcoal, and diatoms records are less precise than the lithologic record, we refer only to median calibrated radiocarbon ages.

The late-glacial period at Rush, Twin Buttes, and Cygnet lakes was initially dominated by nonarboreal pollen taxa [46 to 76% at Rush, 69 to 76% at Twin Buttes, 60 to 80% at Cygnet (9)], including *Artemisia*, Poaceae, and various herbs, along with low percentages of arboreal taxa (*Juniperus*, *Salix*, and *Betula*) (Fig. 2*A* and *SI Appendix*, Fig. S3). Comparison with modern pollen spectra suggests that the early deglacial landscape supported cold steppe vegetation with sagebrush and juniper in dry settings and willow and birch in wet habitats (52). Early postglacial charcoal levels were low (<1.5 particles cm^{-2} y^{-1}), indicating few wildfires during a time of limited woody fuel (Fig. 2*B*).

Late-glacial diatom assemblages from Rush Lake show early dominance of planktonic phosphorous specialists (up to 72%) (*Stephanodiscus minutulus*, *Fragilaria tenera*, and *Cyclotella distinguenda*) and small, colonial Fragilariaceae tychoplankton (*Staurosira construens* var. *venter*) (*SI Appendix*, Fig. S4). Overall, the diatom assemblage describes a relatively shallow lake, similar to present, receiving abundant nutrients (Fig. 2*C*). A pulse of *C. distinguenda* (up to 72%) from 12.7 to 12.0 ka (4.16 to 3.72 m depth) indicates a brief interval of alkaline water composition following a peak in relative As concentration at 12.8 to 12.7 ka (4.30 to 4.18 m depth) (Fig. 2*D*) that implies increased hydrothermal input.

As early as 12.8 ka at Rush Lake and 11.5 ka at Cygnet Lake, increased percentages of *Pinus* pollen (40 to 75%) mark the initial colonization of pine (Fig. 2*A*). Both *Pinus* subgenus *Pinus* pollen, attributed to lodgepole pine, and *P.* subgenus *Strobus* pollen, from whitebark or limber pine, were likely present in the early forest from ca. 12.8 to 7 ka. The dominance of *P*. subgenus *Pinus* pollen after 11 ka denotes the time when lodgepole pine forest covered Lower Geyser Basin, the Central Plateau, and probably most of the Yellowstone Plateau volcanic field. Greater forest cover provided ample woody fuel biomass for wildfires during the late-glacial to early-Holocene transition, as evidenced by increased CHAR at Rush, Goose, Harlequin, and Cygnet (53) lakes after 12 ka (Fig. 2*B*).

The diatom record at Rush Lake was dominated by benthic species (average 19%) (*Navicula wildii*, *Grunowia solgensis*) and small, colonial tychoplankton (*S. construens* var. *venter*) (average 37%) after 11.6 ka (Fig. 2*C* and *SI Appendix*, Fig. S4). These taxa are limited by nutrient availability and indicate circumneutral pH. The presence of *Epithemia gibba* at Rush Lake, and the abundance of *Diatoma moniliformis* at Goose Lake suggests shallow, low-nutrient conditions and warm water temperatures in the early Holocene (20, 54).

The middle-Holocene period featured high percentages of *Pinus* subgenus *Pinus* pollen at Cygnet, Rush, Goose, and Feather lakes and low values of *Artemisia*, Poaceae, and other herbs, indicating sustained lodgepole pine forest (Fig. 2*A*). High CHAR at all lakes from 8 to 4 ka (up to 20 particles cm^{-2} y^{-1}) (Fig. 2*B*) are evidence of frequent stand-replacement fires at that time. Today, the serotinous cones of lodgepole pine release their seeds when subjected to high heat, allowing pine forests to regenerate rapidly after intense wildfire (55), and this positive forest-fire feedback undoubtedly helped maintain lodgepole pine forest in the past. During the middle Holocene, elevated fire activity likely supported dense pine stands similar to those that developed after the 1988 Yellowstone fires (28).

Rush Lake diatom composition changed little in the middle Holocene, indicating persistent nutrient limitations and warm, shallow water (Fig. 2*C* and *SI Appendix*, Fig. S4). In Goose Lake, loss of planktic *Cyclotella meneghiniana* at the expense of benthic taxa also implies low nutrient availability and warm, shallow water (20). Most of the taxa have wide pH and temperature tolerances at present consistent with persistent hydrothermal input to the lake. Diatom samples dating to 6.54 and 5.5 ka from Feather Lake indicate relatively shallow, moderately alkaline water (*SI Appendix*).

In the late Holocene, *Pinus* subgenus *Pinus* pollen continued to dominate the assemblage at Rush, Cygnet, Goose, and Feather lakes (Fig. 2*A*). At Goose and Rush lakes, *Pinus* percentages decreased slightly after 4 ka at the expense of *Artemisia* and Poaceae values, possibly marking local expansion of thermal grassland. A decline in CHAR after 3.5 ka indicates less wildfire activity than before (Fig. 2*B*).

The late-Holocene diatom assemblage (4.6 ka–present) at Rush Lake indicates renewed phosphorous enrichment and shallow water, especially in the last 3,000 years (Fig. 2*C*) (*SI Appendix*, Fig. S4). *Diatoma moniliformis* percentages declined at Goose Lake after 3.8 ka suggesting less hydrothermal input than before (20). Diatom samples from Feather Lake at 2.4 ka and 1.9 ka imply lower nutrient conditions than before (*SI Appendix*).

It is interesting that inferred changes in the vegetation and limnobiota are not consistently matched by changes in the relative concentrations of As and Cs, which vary among sites and through time (Fig. 2*D*). Steady presence of As and Cs at all sites points to sustained hydrothermal input since lake formation but levels of enrichment varied. Notably high As levels prior to 12.5 ka at Rush Lake, prior to 3.8 ka at Goose Lake, and after 3.3 ka at Feather Lake suggest periods of above-present, local hydrothermal enrichment.

Climatic and Nonclimatic Drivers of Postglacial Ecological Change in the Yellowstone Region. Over timescales of centuries to millennia, the postglacial climate history of western North America has largely been determined by ablation of the Laurentide and Cordilleran ice sheets, amplification of the seasonal cycle of insolation, and rising levels of atmospheric trace gases, primarily CO_2 (ppmV ranged from 220 at 15 ka to 275 ppm at 0 ka) (56). Amplification of the seasonal cycle of insolation from 12 to 6 ka in northwestern North America, including the Yellowstone region (Fig. 3*A*), directly resulted in warmer summers, colder winters, and changes in surface energy balance and water budgets. Indirectly, higher summer insolation strengthened the northeastern Pacific subtropical high-pressure system (*SI Appendix*, Fig. S5*A*), suppressing precipitation and increasing evapotranspiration (27). As insolation decreased in summer and increased in winter in the late Holocene, summers became cooler and winters warmer, and effectively wetter conditions prevailed.

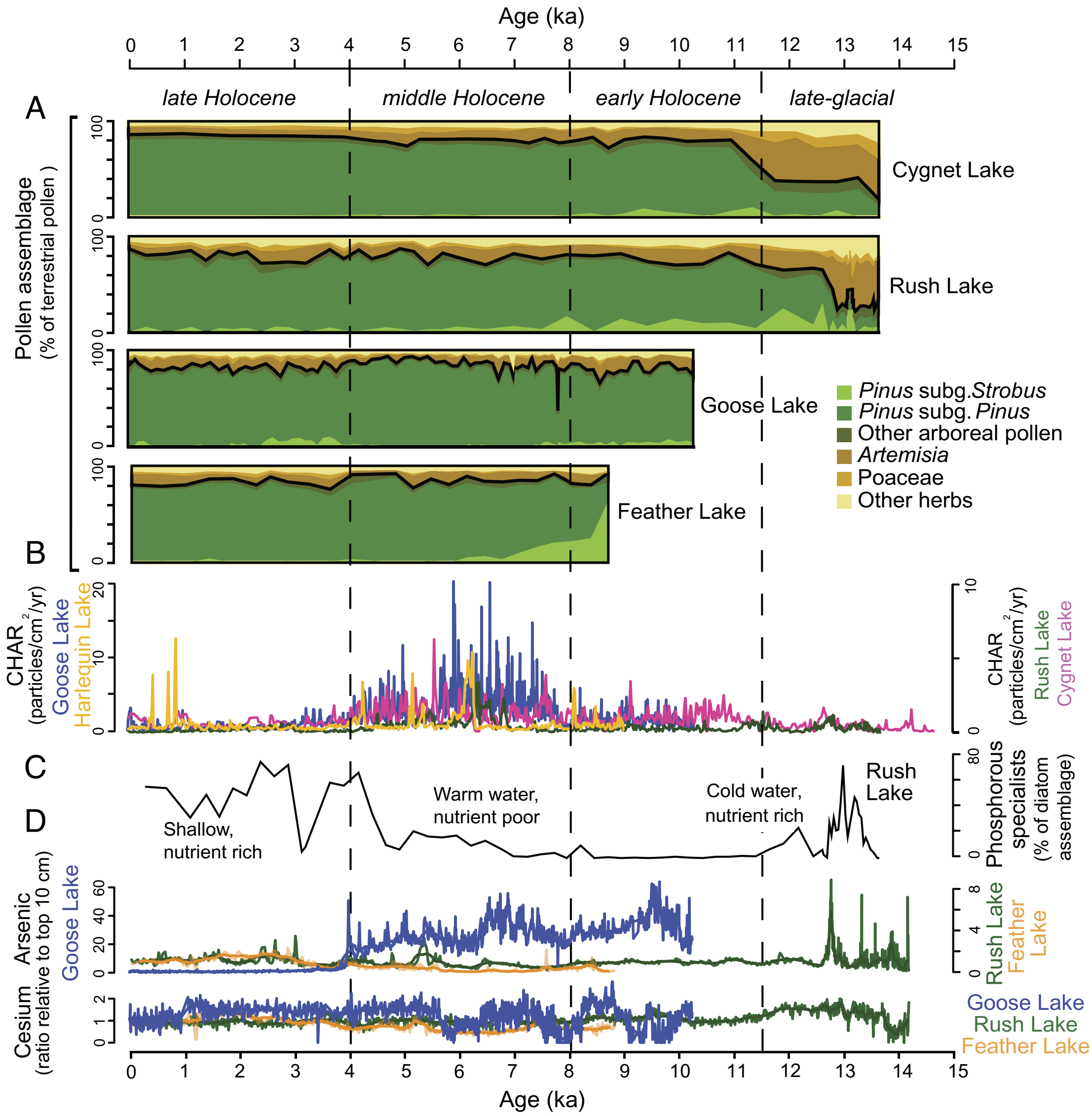

Fig. 2. Paleoenvironmental data from Lower Geyser Basin. (*A*) Pollen records from Cygnet, Rush, Goose, and Feather lakes showing vegetation development. (*B*) Charcoal accumulation rates (CHAR) from Goose, Rush, Cygnet, and Harlequin lakes registering changes in fire activity. (*C*) Stratigraphy of phosphorous specialists in the Rush Lake diatoms record indicating nutrient levels. (*D*) Arsenic (As) and Cesium (Cs) ratios showing hydrothermal activity relative to top 10 cm of core.

Anomalies for the 12 to 0 ka, 9 to 0 ka, 6 to 0 ka, and 3 to 0 ka simulations for the Yellowstone region illustrate how climate conditions during the late-glacial and early, middle, and late Holocene differed from those of the pre-Industrial present (0 ka) (Fig. 4). For Lower Geyser Basin, annual precipitation was less at 12 ka (−216 mm, −16%) and 9 ka (−95 mm, −7%) relative to 0 ka (Table 2). Annual effective moisture (P–E) anomalies for 12 ka (−96 mm, −23%), 9 ka (−136 mm, −32%), and 6 ka (−63 mm, −15%) indicate drier conditions than at 3 or 0 ka (Fig. 4*A* and Table 2). Snowpack (April 1 SWE) from 12 to 6 ka was higher than 0 ka at high and low elevations in the region but close to or lower than 0 ka levels in Lower Geyser Basin (Fig. 4*B* and Table 2). From 12 to 6 ka, summers were warmer with peak July–September temperature anomalies at 12 ka (2.6 °C) and 9 ka (2.7 °C) and lower effective moisture (P–E) at 12 ka (−66 mm), 9 ka (−110 mm), and 6 ka (−74 mm) (Fig. 4*C* and Table 2). Warmer, drier atmospheric conditions were associated with much higher July–September VPD at 12 ka [1.6 hectopascal (hPa), 56%], 9 ka (1.4 hPa, 48%), and 6 ka (0.9 hPa, 29%), compared with 0 ka (Fig. 4*D* and Table 2).

Rising summer insolation and temperature in the late-glacial period led to rapid ice recession and the resulting high levels of cold meltwater likely increased hydrothermal activity. It has been suggested that deglacial breaching of an ice-dammed lake in Lower Geyser Basin caused a rapid drop in confining pressure and the ensuing hydrothermal explosions created Pocket Basin, the landslide and hydrothermal craters atop Twin Buttes (29), and the Rush Lake basin (30). The basal ages of Rush and Twin Butte lakes corroborate a late-glacial origin. Similarly, travertine rather than silica sinter was deposited from 13.9 to 13.6 ka and 12.2 to 9.5 ka on the margins of Lower Geyser Basin in response to large volumes of cold groundwater that increased the chemical weathering of surficial sediments (58). High groundwater recharge from snowmelt may also have triggered the hydrothermal explosions that formed Goose Lake at >10.3 ka and Feather Lake at 8.8 ka.

A lengthening growing season during the late-glacial-to-early-Holocene transition allowed conifers to move from glacial refugia outside the former ice margin into deglaciated terrain. Colonization of pine occurred at 12.8 ka at Rush Lake and ca. 11.5 ka at Cygnet Lake (Fig. 3*B*). The earlier establishment of pine at Rush Lake

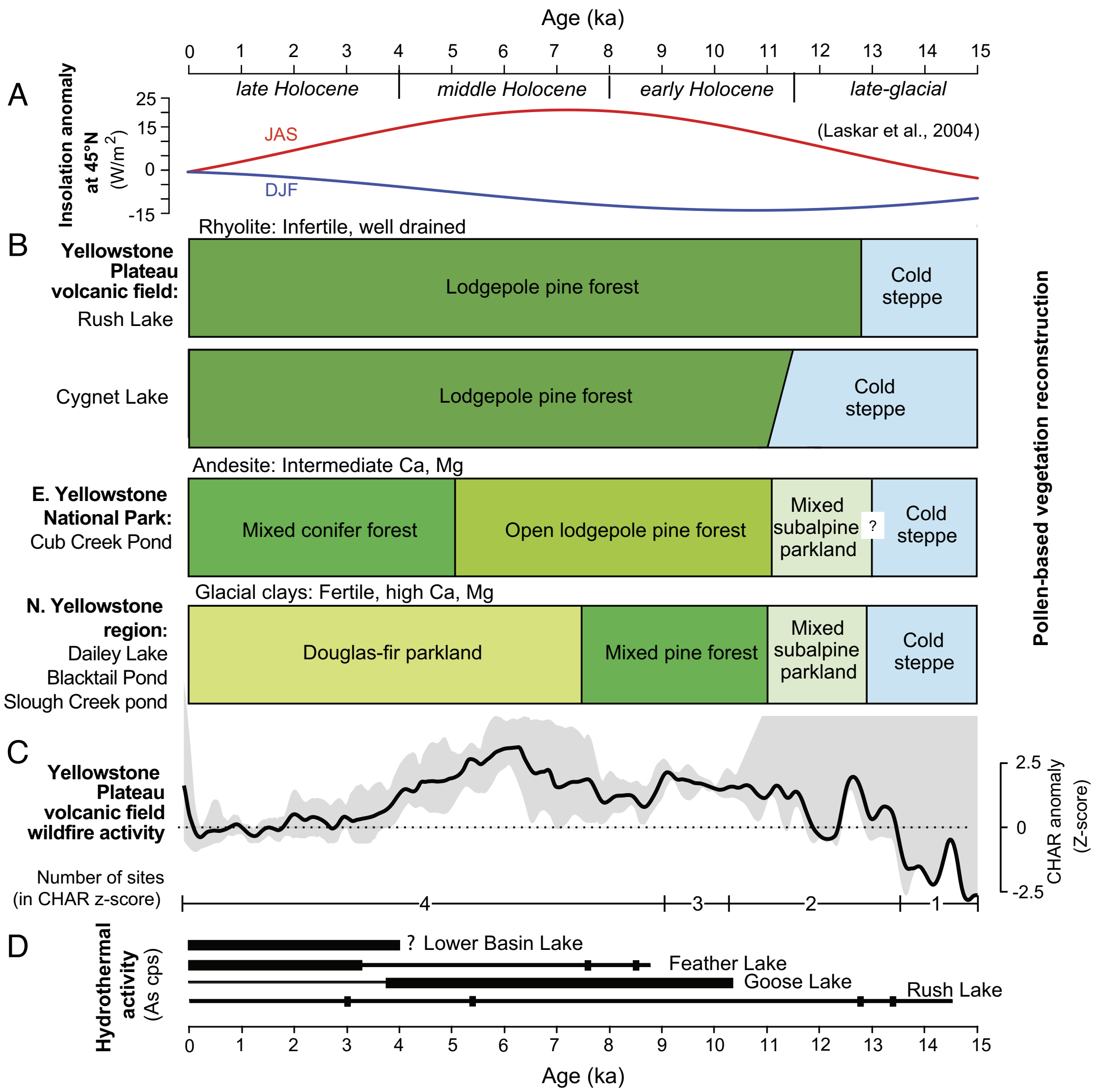

Fig. 3. Comparison of insolation anomaly and paleoenvironmental reconstructions for Lower Geyser Basin and the Yellowstone region. (*A*) Insolation anomaly for 45°N in August (height of fire season) (57). (*B*) Pollen-based vegetation reconstructions in the Yellowstone region. (*C*) Anomalies of standardized charcoal accumulation rates (CHAR) showing variations in wildfire activity on the Yellowstone Plateau volcanic field (gray shading represents 95% confidence interval) and number of records in the anomaly calculation. (*D*) origination age and periods of hydrothermal activity as inferred sedimentary arsenic (As) data. Thick bars indicate higher-than-present As concentrations.

than at Cygnet Lake may be explained by Lower Geyser Basin's geothermally warmed substrates, relatively low elevation, and proximity to glacial refugia outside western ice margins compared to the Central Plateau. Lodgepole pine, and to a lesser extent whitebark and/or limber pine, were present in forests in the volcanic field from ca. 12.8 to 7 ka, with the white pines growing on the most fertile substrates.

While lodgepole pine was favored over other conifers on rhyolitic substrates, mesophytic conifers established on more-nutrient-rich substrates (59) (Fig. 3*B*). Nonrhyolite sites from the Absaroka Range in eastern Yellowstone National Park [Cub Creek Pond (9)] and the northern Yellowstone region [Dailey Lake, Blacktail Pond, and Slough Creek pond (Fig. 1 *B* and *C*) (11)] record a late-glacial transition from steppe to subalpine parkland of Engelmann spruce at ca. 13 ka followed by the addition of subalpine fir and white pines after ca. 12.3 ka. Positive charcoal anomalies at this time suggest that stand-replacing wildfires accompanied the increase in woody fuels, decrease in annual effective moisture, and warming summer temperatures (Fig. 3*C*).

The consequences of warmer, effectively drier summers in the early and middle Holocene are well documented in paleoenvironmental records throughout the northwestern United States (e.g., refs. 60 and 61). In the Yellowstone region, these conditions explain higher-than-present evaporation in Yellowstone Lake prior to 7 ka (10), lower lake levels across the region prior to 6 ka (62), and low ice-accretion rates in the Beartooth Plateau in northwestern Wyoming prior to 3.9 ka (63). Warmer, drier summers compared to 0 ka also explain the low mobilization of nutrients, high water temperatures, and low lake levels at Rush Lake from 12.5 to 4.5 ka. Similarly, early- and middle-Holocene diatom assemblages at Goose and Feather lakes indicate nutrient-depleted warm water, reflecting both climatic and hydrothermal influences on limnological conditions.

Currently, area burned in the western United States is positively correlated with summer shortwave radiation, 500 hPa height, air temperature, and VPD and negatively correlated with effective moisture (45, 64). In Lower Geyser Basin, increases in July–September VPD at 12, 9, and 6 ka compared to 0 ka (56% at 12 ka, 48% at 9 ka, and 29% at 6 ka) (Fig. 4*D* and Table 2) help explain

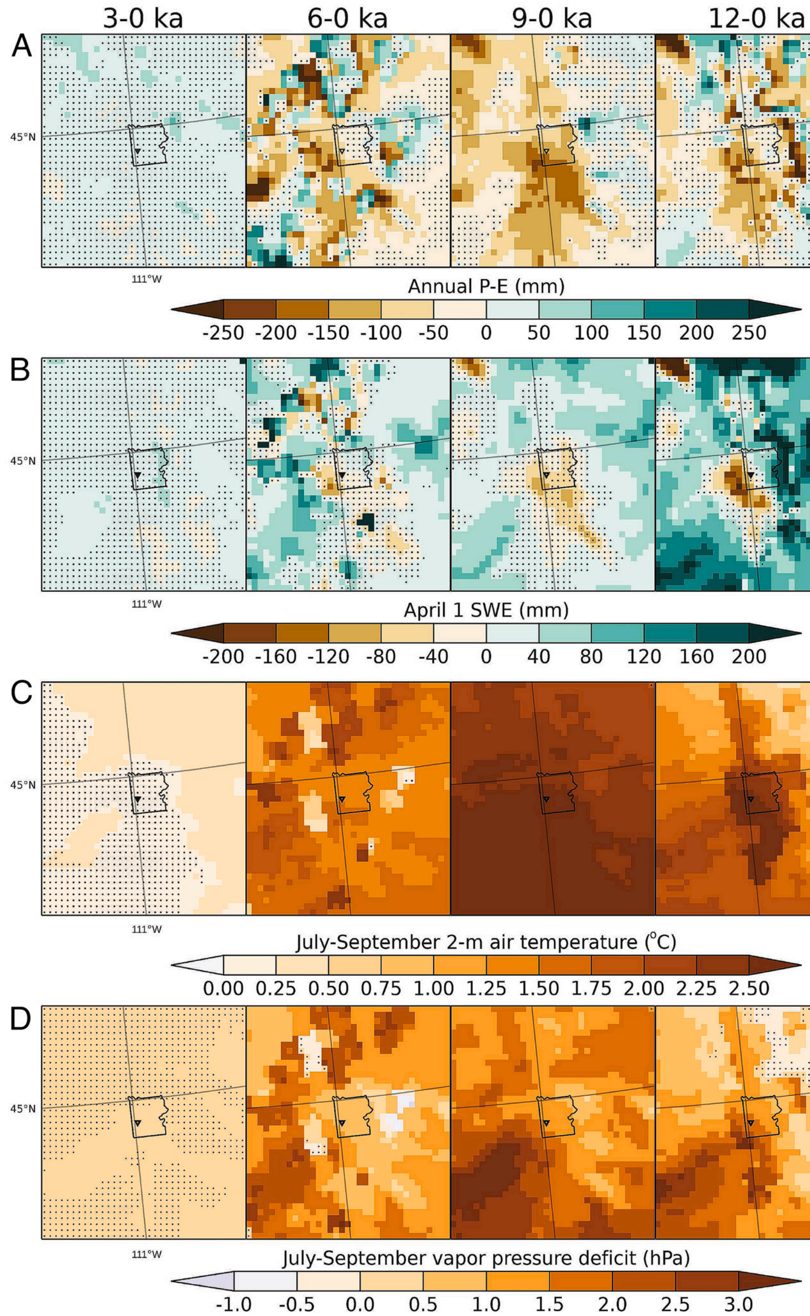

Fig. 4. Maps showing simulated Holocene climate anomalies for the Yellowstone region on the 15-km Lambert Conformal projection of the climate model. Yellowstone National Park (black outline), and Lower Geyser Basin (black triangle) are shown. (*A*) Effective moisture [P−E: annual precipitation minus evaporation (mm)]. (*B*) Snowpack [April 1st snow-water equivalent (SWE) (mm)]. (*C*) July–September 2-m air temperature (°C). (*D*) July–September vapor pressure deficit (hPa). Mapped values are differences between indicated period and 0 ka (pre-Industrial present). Stippling indicates lack of significance of the changes at the 95th percentile based on a *t*-means test.

increased levels of biomass burning from the late-glacial to middle Holocene. Noteworthy is that the highest wildfire activity occurred in the middle Holocene (Fig. 3*C*), even though the VPD anomaly at 9 ka is higher than at 6 ka. We suggest that cooler, wetter spring conditions at 6 ka, brought on by declining spring insolation, may explain the difference, because moisture early in the growing season favors fine-fuel development. Abundant grasses and forbs would have established during cool middle-Holocene springs and dried quickly with high July–September temperature and VPD, thus promoting the spread of large, late-summer wildfires as occurs today (45, 65).

Climate anomalies for 3 ka indicate that declining summer insolation in the late Holocene brought increases in annual precipitation, annual and summer effective moisture (P−E), and snowpack (April 1 SWE), as well as decreased summer temperatures and VPD compared to previous periods (Fig. 4). The shift to cooler, wetter conditions is evident in Lower Geyser Basin. At Rush Lake, phosphorous-sensitive diatoms imply cooler or longer springs than before (Fig. 2*C*). The diatom assemblage and sediment chemistry at Goose Lake show evidence of greater freshwater input (20). The inferred origin of Lower Basin Lake in the late Holocene is consistent with greater groundwater input to the thermal area, also during a time of higher snowpack. Other paleoenvironmental records in the Yellowstone region similarly track the trend toward cooler, wetter conditions in the late Holocene: renewed glacial activity in the Teton Range occurred from 6 to

Table 2. Simulated climate variables for LGB

	3 to 0 ka*	6 to 0 ka	9 to 0 ka	12 to 0 ka
Annual precipitation†	26 mm, 2%	−36 mm, −3%	**−95 mm‡, −7%**	**−216 mm, −16%**
Annual effective* moisture (P−E)	**27 mm, 6%**	**−63 mm, −15%**	−136 mm, −32%	**−96 mm, −23%**
April 1st snow water equivalent (SWE)†	24 mm, 3%	−19 mm, −2%	**−49 mm, −6%**	−19 mm, −2%
July-September 2-m air temperature†,§	**0.2 °C**	**1.5 °C**	**2.7 °C**	**2.6 °C**
July-September†,§ effective moisture (P−E)	−17 mm, −8%	**−74 mm, −36%**	**−110 mm, −54%**	**−66 mm, −33%**
July-September 2-m vapor pressure deficit (VPD)†,§	**0.2 hPa, 5%**	**0.9 hPa, 29%**	**1.4 hPa, 48%**	**1.6 hPa, 56%**

*0 ka is pre-Industrial present.
†Values for precipitation, P−E, SWE, and VPD are anomalies from 0 ka and percent change.
‡Bold indicates statistical significance at the $P < 0.05$ level based on a t means test.
§July-September simulated values are averaged over June 21 to September 20.

2.4 ka and after 1 ka (66), ice-accretion rates on the Beartooth Plateau increased after 3.9 ka (63), Yellowstone Lake evapotranspiration declined after 7 ka and again at 3.5 ka (10), and upper treelike was lowered and lake levels rose on the Beartooth Plateau (67).

Lodgepole pine forest continued to dominate the late-Holocene vegetation of the Yellowstone Plateau volcanic field, although thermal grassland may have expanded somewhat in Lower Geyser Basin. Wildfire activity substantially declined after 4 ka with the onset of climate conditions less favorable for burning (Fig. 3*C*). Mesophytic forest of spruce and subalpine fir dominated in the nonrhyolite regions of southern and eastern Yellowstone National Park (9), replacing open pine-dominated forest of the early Holocene. Parkland of Douglas-fir (*Pseudotsuga menziesii*) replaced a mixed pine forest in northern Yellowstone after 7.5 ka (27) (Fig. 3*B*).

In sum, the postglacial environmental history of Lower Geyser Basin has been shaped by the interaction of climate and geology through time. Variations in the seasonal cycle of insolation that govern long-term shifts in temperature, available moisture, and snowpack triggered both abiotic and biotic responses. As part of deglaciation, increased water availability was likely an important mechanism for the hydrothermal explosions that led to the formation of Rush, Twin Buttes, and Goose lakes (Fig. 3*D*). Increased snowpack and effective moisture also may have triggered the hydrothermal activity that formed Lower Basin Lake in the late Holocene. Likewise, the limnobiota was strongly influenced by temperature and effective moisture, which shaped nutrient levels, water temperature, and water level. Highest wildfire activity occurred when summer temperatures and VPDs were highest in the early and middle Holocene and declined during the cooler, wetter late Holocene. Lodgepole pine forests were established on the Yellowstone Plateau volcanic field by 11 ka when rising temperatures enabled pine to colonize areas previously covered by steppe. These forests were, and still are, well adapted to the infertile, dry rhyolite substrates of the volcanic field, and despite pronounced variations in climate and wildfire activity in the Holocene, they have persisted to the present with little change.

Our findings suggest that the climatic and hydrothermal controls that maintain the present-day ecosystem dynamics of the geyser basins of Yellowstone have operated since deglaciation. While changes in insolation will be negligible over the next century, continued warming from atmospheric greenhouse gases will alter these dynamics, especially as the region warms beyond temperatures seen in the last 18,000 years (68). Model projections for the Yellowstone region suggest that temperatures 2 to 3 °C warmer than 0 ka will reduce snowpack by 30%, and earlier snowmelt will lead to significant late-summer drought and wildfires by midcentury (68, 69). Reduced snowpack will also likely dampen hydrothermal recharge as occurred in the past. A yet unanswered question is whether the soil characteristics of rhyolite, which have maintained lodgepole pine forests for millennia, will remain a dominant stabilizer in the future, overriding the effects of climate and wildfire that might otherwise change vegetation composition.

Materials and Methods

Sediment cores were collected with a modified Livingstone corer (70) from an anchored floating platform in the center of each lake (Table 1 for site information). Cores were longitudinally split, imaged, and analyzed for physical parameters (magnetic susceptibility, color, reflectance, density, profile) at 0.5 cm resolution at the Continental Scientific Drilling (CSD) Facility (University of Minnesota Twin Cities) for initial core description. Characterization of fine sediments was done through smear slide analysis.

XRF was measured every 0.5 cm for bulk elemental geochemistry at the Large Lakes Observatory (LLO, University of Minnesota-Duluth) and the USGS Pacific Coastal and Marine Science Center. LLO XRF data were collected with a ITRAX XRF core scanner using 30-s count times, 30 kV X-ray voltage, and an X-ray current of 20 mA. We normalized to surface (top 10-cm core depth) XRF values to display As and Cs trends as either enriched or depleted relative to recent concentrations. Normalized values were smoothed using a 20-sample (10 cm depth) moving average. The $\delta^{13}C_{sediment}$ determinations on bulk sediments were carried out at the U.S. Geological Survey, Reston Stable Isotope Laboratory.

A chronology for the cores was provided through accelerator mass spectrometry radiocarbon dating of charcoal, terrestrial plant fragments, and bulk sediments at the National Ocean Sciences Accelerator Mass Spectrometry Facility in Woods Hole, Massachusetts (*SI Appendix*, Table S1). Radiocarbon samples were washed with distilled water, cleaned with a dissecting needle under a stereomicroscope, and treated with acid–base–acid washes. Where sufficiently large, samples were split for $\delta^{13}C$ analysis to assess carbon provenance. Single-grain microbe analysis of glass-bearing minerals in the volcanic ash layers was used to identify Mazama and Glacier Peak ashes; these analyses were undertaken at the New Mexico Bureau of Geology and Mineral Resources.

Following standard procedures (71), pollen analysis from Rush and Feather lakes was conducted at approximately 16-cm resolution on ~0.5 cm^3 subsamples. At least 300 terrestrial pollen grains were identified at magnifications of 400 to 1,000× to the lowest possible taxonomic level based on relevant atlases [e.g., (72)] and modern reference collections. *Pinus* grains with visible, intact distal membranes were assigned to *Pinus* subgen. *Pinus* (*P. contorta*) and *P.* subgen. *Strobus* (*P. albicaulis* or *P. flexilis*). Terrestrial pollen percentages were based on total terrestrial pollen as the denominator, and aquatic pollen and spore percentages were calculated using the total palynomorph sum. Percentages of *Pinus* subg *Strobus* and *P.* subg *Pinus* pollen were based on the ratio of identifiable *Pinus* pollen grains applied to the total *Pinus*.

Samples of ~2 cm^3 were collected for charcoal analysis at contiguous 0.5- and 1.0-cm intervals at Rush and Harlequin lakes to reconstruct wildfire history. Charcoal particles >125 μm in diameter were extracted and counted according to standard methodology to analyze long-term trends in charcoal abundance (43). CHAR (particles $cm^{-2}\,y^{-1}$) were calculated with CharAnalysis software for MatLab (73) and interpreted as an indicator of wildfire activity or overall time-averaged biomass burned. To standardize new and published data for the composite record (Fig. 3*D*), CHAR anomalies were calculated using statistical minmax, Box-Cox, and finally Z-score transformations.

Diatom samples of ~0.5 cm^3 volume were washed with 30% wt/vol hydrogen peroxide to remove organic matter (74); the residue was mounted with a Naphrax optical adhesive. Diatom valves were identified using regional taxonomic resources (75, 76). A total of 300 diatom valves were enumerated per slide and analyzed as a percent of the diatom sum. Lake conditions inferred from the diatom community were based on species-level autecology.

We downscaled global climate simulations previously conducted with the GENMOM coupled atmosphere-ocean general circulation model at T31 resolution (~3.71° latitude × 3.75° longitude) (77) by progressively nesting 50- and 15-km configurations of the hydrostatic version of the RegCM5 regional climate model (44) over western North America (78). The 50-km model domain retains key circulation features, and the smaller 15-km domain captures important topographic controls of regional climate. The global simulations were run to equilibrium at 3,000-year intervals from 21 to 0 ka using time-dependent boundary conditions, including insolation, atmospheric greenhouse gas concentrations, ice-sheet extent and height, and sea level. RegCM5 was first run over a 50-km horizontal grid with 23 vertical atmospheric levels coupled with the Biosphere-Atmosphere Transfer Scheme (BATS1E) surface-physics model (79, 80). These boundary conditions were then prescribed in the regional model along with ICE6G Laurentide and Cordilleran ice-sheet reconstructions and changing paleovegetation. Past vegetation (*SI Appendix*, Fig. S5*B*) was specified in the model by cross-referencing reconstructed vegetation types with the 20 available land-use classes in BATS1E, which assigns physical characteristics (e.g., albedo, aerodynamical roughness, fractional cover, stomatal resistance, soil texture, and color).

The 50-km simulations were driven by 105 years of continuous 6-h lateral boundary conditions (vertical profiles of atmospheric temperature, wind, humidity, surface pressure, and sea-surface temperature) derived from the GENMOM simulations. We then ran the 15-km model over a smaller domain for the same 105 years using boundary conditions derived from the 50-km run. We used the last 100 years of the 15-km RegCM5 simulations to exclude model spin-up.

VPD is computed from the model output as

$$\mathrm{VPD} = (1 - rh)0.168e^{17.27T/237.3T},$$

where *rh* is relative humidity at 2 m and *T* is the temperature 2-m air temperature in °C.

The Laskar et al. (57) insolation data for the summer wildfire season (Fig. 3*A*) span June 21 through September 20, and summer model data were averaged over the same days of the year.

Data, Materials, and Software Availability. Pollen, charcoal, diatom, XRF data have been deposited in the Neotoma Paleoecology Database (81–89). All other data are included in the manuscript and/or *SI Appendix*. Previously published data were used for this work [Model data: (78), Goose Lake data: (20)].

ACKNOWLEDGMENTS. Funding was provided by U.S. NSF Grant EAR-2149482 to D.B.M. and C.W. Field work was conducted under Yellowstone National Park permit YELL-SCI-0009. We received field and laboratory help from A. Carlson, R. Chidlow, J. Crozier, S. Mark, B. Rowe, C. Smythies, H. Webb, S. Wing, and C. Worrell. We thank N. Iverson at the New Mexico Bureau of Mining and Technology for tephra identifications; D. Mogk and S. Zacher at the Montana State University Imaging and Chemical Analysis Laboratory; and J. Falgout, J. Gordon, L. Lopaka, and B. Williams of the U.S. Geological Survey Advanced Research Computing group and the Hovenweep Supercomputer facility. Reviews from S. Fritz, J. Pierce, and G. Pederson greatly improved the paper. Any use of trade, firm, or product names is for descriptive purposes and does not imply endorsement by the U.S. Government.

Author affiliations: [a]Department of Earth Sciences and Institute on Ecosystems, Montana State University, Bozeman MT 59717; [b]Institute on Ecosystems, Montana State University, Bozeman, MT 59717; [c]Burke Museum of Natural History and Culture, University of Washington, Seattle, WA 98195; [d]College of Earth, Ocean and Atmospheric Sciences, Oregon State University, Corvallis, OR 97331; [e]California Volcano Observatory, U.S. Geological Survey, Moffett Field, CA 94035; [f]Niswander Department of Biology, Manchester University, North Manchester, IN 46845; [g]Department of Geosciences, Colorado State University, Fort Collins, CO 80523; and [h]U.S. Geological Survey, Corvallis, OR 97331

Author contributions: C.W., C.M.S., and S.W.H. designed research; C.W., C.M.S., S.W.H., S.H., M.A., S.R.B., L.N.H., J.R.A., K.B., and J.S. performed research; C.W., C.M.S., S.W.H., S.H., M.A., and S.R.B. analyzed data; and C.W., C.M.S., S.W.H., S.H., M.A., S.R.B., and D.B.M. wrote the paper.

1. R. L. Christiansen *et al.*, "Preliminary assessment of volcanic and hydrothermal hazards in Yellowstone National Park and vicinity" (USGS Open-File Report 2007-1071, U.S. Geological Survey, 2007), p. 94.
2. N. E. Matthews, J. A. Vazquez, A. T. Calvert, Age of the Lava Creek supereruption and magma chamber assembly at Yellowstone based on $^{40}Ar/^{39}Ar$ and U-Pb dating of sanidine and zircon crystals. *Geochem. Geophys. Geosyst.* **16**, 2508–2528 (2015).
3. M. E. Stelten, N. Thomas, A. Pivarunas, D. Champion, Spatio-temporal clustering of post-caldera eruptions at Yellowstone caldera: Implications for volcanic hazards and pre-eruptive magma reservoir configuration. *Bull. Volcanol.* **85**, 55 (2023).
4. R. O. Fournier, Geochemistry and dynamics of the Yellowstone National Park hydrothermal system. *Annu. Rev. Earth Planet. Sci.* **17**, 13–53 (1989).
5. S. Hurwitz, J. B. Lowenstern, Dynamics of the Yellowstone hydrothermal system. *Rev. Geophys.* **52**, 375–411 (2014).
6. D. G. Despain, *Yellowstone Vegetation: Consequences of Environment and History in a Natural Setting* (Robert Rinehart Publishers, 1990), p. 238.
7. R. G. Vaughan, H. Heasler, C. Jaworowski, J. B. Lowenstern, L. P. Keszthelyi, "Provisional maps of thermal areas in Yellowstone National Park, based on satellite thermal infrared imaging and field observations" (USGS Scientific Investigations Report 2014-5137, 2013), 22pp.
8. R. L. Christiansen, "The quaternary and pliocene Yellowstone plateau volcanic field of Wyoming, Idaho, and Montana" (U.S. Geological Survey Professional Paper 729, U.S. Geological Survey, 2001). p. 145. https://doi.org/10.3133/pp729G. Accessed 27 July 2026.
9. C. Whitlock, Postglacial vegetation and climate of Grand Teton and southern Yellowstone National Parks. *Ecol. Monogr.* **63**, 173–198 (1993).
10. S. R. Brown *et al.*, Multi-proxy record of Holocene paleoenvironmental conditions from Yellowstone Lake, Wyoming, United States. *Quat. Sci. Rev.* **274**, 107275 (2021).
11. T. R. Krause, C. Whitlock, Climatic and non-climatic controls shaping early postglacial conifer history in the northern Greater Yellowstone Ecosystem, USA. *J. Quat. Sci.* **32**, 1022–1036 (2017).
12. S. Husen, R. Taylor, R. B. Smith, H. Healser, Changes in geyser eruption behavior and remotely triggered seismicity in Yellowstone National Park produced by the 2002 M 7.9 Denali fault earthquake, Alaska. *Geology* **32**, 537–540 (2004).
13. S. Hurwitz *et al.*, Yellowstone's Old Faithful Geyser shut down by a severe 13th century drought. *Geophys. Res. Lett.* **47**, e2020GL089871 (2020).
14. S. Hurwitz *et al.*, The relation between decadal droughts and eruptions of Steamboat Geyser in Yellowstone National Park, United States. *Geochem. Geophys. Geosyst.* **24**, e2023GC010988 (2023).
15. S. Hurwitz, A. Kumar, R. Taylor, H. Heasler, Climate-induced variations of geyser periodicity in Yellowstone National Park, United States. *Geology* **36**, 451–454 (2008).
16. G. T. Pederson *et al.*, The unusual nature of recent snowpack declines in the North American Cordillera. *Science* **333**, 332–335 (2011).
17. S. Hurwitz *et al.*, The systematics of stable hydrogen (δ^2H) and oxygen ($\delta^{18}O$) Isotopes and tritium (^3H) in the Hydrothermal System of the Yellowstone Plateau Volcanic Field, USA. *Geochem. Geophys. Geosyst.* **26**, e2025GC012230 (2025).
18. C. E. Briles, C. Whitlock, C. N. Skinner, J. Mohr, Holocene forest development and maintenance on different substrates in the Klamath Mountains, northern California, United States. *Ecology* **92**, 590–601 (2011).
19. L. B. Brubaker, Postglacial forest patterns associated with till and outwash in northcentral Upper Michigan. *Quat. Res.* **5**, 499–527 (1975).
20. C. M. Schiller, C. Whitlock, S. R. Brown, Holocene geo-ecological evolution of lower geyser basin, Yellowstone National Park (United States). *Quat. Res.* **105**, 201–217 (2022).
21. L. J. Muffler, D. E. White, A. H. Truesdell, R. O. Fournier, "Geologic map of Lower Geyser Basin, Yellowstone National Park, Wyoming" (USGS Miscellaneous Investigations Series Map I-1373, U.S. Geological Survey, 1982).
22. J. M. Licciardi, K. L. Pierce, History and dynamics of the Greater Yellowstone Glacial System during the last two glaciations. *Quat. Sci. Rev.* **200**, 1–33 (2018).
23. J. S. Sheppard, *The Influence of Geothermal Temperature Gradients upon Vegetation Patterns in Yellowstone National Park* (Colorado State University, Fort Collins, CO, 1971), p. 157.
24. A. Rodman, H. F. Shovic, D. Thoma, "Soils of Yellowstone National Park" (Tech. Rep. YCR-HRSR-96-2, Yellowstone Center for Resources, Yellowstone National Park, 1996), p. 293. https://npshistory.com/publications/yell/ycr/ycr-nrsr-96-2.pdf. Accessed 27 July 2026.
25. PRISM Climate Group, 30-year normals. (2004). https://prism.oregonstate.edu. Accessed 27 July 2026.
26. C. J. Mock, Climatic controls and spatial variations of precipitation in the western United States. *J. Clim.* **9**, 1111–1125 (1996).
27. C. Whitlock, P. J. Bartlein, Spatial variations of Holocene climatic change in the Yellowstone region. *Quat. Res.* **39**, 231–238 (1993).
28. W. H. Romme *et al.*, Twenty years after the 1988 Yellowstone fires: Lessons about disturbance and ecosystems. *Ecosystems* **14**, 1196–1215 (2011).
29. L. J. P. Muffler, D. E. White, A. H. Truesdell, Hydrothermal explosion craters in Yellowstone National Park. *Geol. Soc. Am. Bull.* **82**, 723–740 (1971).
30. L. A. Morgan, W. C. Shanks, K. L. Pierce, Hydrothermal processes above the Yellowstone magma chamber: Large hydrothermal systems and large hydrothermal explosions. *Geol. Soc. Am. Spec. Pap.* **429**, 95 (2009).
31. A. W. Miller *et al.*, Trophic state evolution of 45 Yellowstone lakes over two decades: Field data and a longitudinal study. *Water* **17**, 1627 (2025).
32. R. B. McCleskey *et al.*, Water-chemistry and isotope data for selected springs, geysers, streams, and rivers in Yellowstone National Park, Wyoming (ver. 2.0, March 2025). *U.S. Geological Survey Data Release*. https://doi.org/10.5066/P92XKJU7. Accessed 27 July 2026.
33. P. Zahajská, S. Opfergelt, S. C. Fritz, J. Stadmark, D. J. Conley, What is diatomite? *Quat. Res.* **2020**, 1–36 (2020).

34. D. Schnurrenberger, J. Russell, K. Kelts, Classification of lacustrine sediments based on sedimentary components. *J. Paleolimnol.* **29**, 141–154 (2003).
35. P. J. Reimer *et al.*, The IntCal20 Northern Hemisphere radiocarbon age calibration curve (0 to 55 cal kBP). *Radiocarbon* **62**, 725–757 (2020).
36. M. Blaauw, J. A. Christen, Flexible paleoclimate age-depth models using an autoregressive gamma process. *Bayesian Anal.* **6**, 457–474 (2011).
37. J. Egan, R. Staff, J. Blackford, A high-precision age estimate of the Holocene plinian eruption of Mount Mazama, Oregon, United States. *Holocene* **25**, 1054–1067 (2015).
38. S. C. Kuehn *et al.*, Major- and trace-element characterization, expanded distribution, and a new chronology for the latest Pleistocene Glacier Peak tephras in western North America. *Quat. Res.* **71**, 201–216 (2009).
39. C. M. Schiller, C. Whitlock, K. L. Elder, N. A. Iverson, M. B. Abbott, Erroneously old radiocarbon ages from terrestrial pollen concentrates in Yellowstone Lake, Wyoming, United States. *Radiocarbon* **63**, 321–342 (2021).
40. R. B. McCleskey *et al.*, The source, fate, and transport of arsenic in the Yellowstone hydrothermal system–An overview. *J. Volcanol. Geotherm. Res.* **432**, 107709 (2022).
41. T. E. C. Keith, J. M. Thompson, R. E. Mays, Selective concentration of cesium in analcime during hydrothermal alteration, Yellowstone National Park, Wyoming. *Geochim. Cosmochim. Acta* **47**, 795–804 (1983).
42. P. E. Higuera, C. Whitlock, J. A. Gage, Linking tree-ring and sediment-charcoal records to reconstruct fire occurrence and area burned in subalpine forests of Yellowstone National Park, United States. *Holocene* **21**, 327–341 (2010).
43. C. Whitlock, C. Larsen, "Charcoal as a fire proxy" in *Tracking Environmental Change Using Lake Sediments*, J. P. Smol, H. J. B. Birks, W. M. Last, R. S. Bradley, K. Alverson, Eds. (Kluwer Academic Publishers, 2001), pp. 75–97.
44. F. Giorgi *et al.*, The fifth generation regional climate modeling system, RegCM5: Description and illustrative examples at parameterized convection and convection-permitting resolutions. *J. Geophys. Res. Atmos.* **128**, e2022JD038199 (2023).
45. S. W. Hostetler, P. J. Bartlein, J. R. Alder, Atmospheric and surface climate associated with 1986–2013 wildfires in North America. *J. Geophys. Res. Biogeosci.* **123**, 1588–1609 (2018).
46. J. T. Abatzoglou, A. P. Williams, Impact of anthropogenic climate change on wildfire across western US forests. *Proc. Natl. Acad. Sci. U.S.A.* **113**, 11770–11775 (2016).
47. L. A. Morgan *et al.*, The dynamic floor of Yellowstone Lake, Wyoming, USA: The last 14 k.y. of hydrothermal explosions, venting, doming, and faulting. *Geol. Soc. Am. Bull.* **134**, 548–574 (2022).
48. K. Cordero, N. D. Brown, L. N. Harrison, S. Hurwitz, Luminescence dating of hydrothermal explosions in the Yellowstone Plateau volcanic field. *Quat. Res.*, 10.1017/qua.2025.10061 (2026). Accessed 27 July 2026.
49. D. E. White, L. J. P. Muffler, A. H. Truesdell, Vapor-dominated hydrothermal systems compared with hot-water systems. *Econ. Geol.* **66**, 75–97 (1971).
50. J. B. Lowenstern, D. Bergfeld, W. C. Evans, A. G. Hunt, Origins of geothermal gases at Yellowstone. *J. Volcanol. Geotherm. Res.* **302**, 87–101 (2015).
51. D. Bergfeld *et al.*, Chemical and isotopic data on gases and waters for thermal and non-thermal features across Yellowstone National Park. *U.S. Geological Survey Data Release*. https://doi.org/10.5066/F7H13105. Accessed 27 July 2026.
52. V. Iglesias, C. Whitlock, T. R. Krause, R. G. Baker, Past vegetation dynamics in the Yellowstone region highlight the vulnerability of mountain systems to climate change. *J. Biogeogr.* **45**, 1768–1780 (2018).
53. S. H. Millspaugh, C. Whitlock, P. J. Bartlein, Variations in fire frequency and climate over the past 17,000 y in central Yellowstone National Park. *Geology* **28**, 211–214 (2000).
54. Th. E. Smith, K. Manoylov, A. Packard, Algal extremophile community persistence from Hot Springs National Park (Arkansas, United States). *Int. J. Algae* **15**, 65–76 (2013).
55. T. Schoennagel, M. G. Turner, W. H. Romme, Influence of fire interval and serotiny on postfire lodgepole pine density in Yellowstone National Park. *Ecology* **84**, 2967–2978 (2003).
56. P. J. Bartlein *et al.*, Paleoclimate simulations for North America over the past 21,000 years: Features of the simulated climate and comparisons with paleoenvironmental data. *Quat. Sci. Rev.* **17**, 549–585 (1998).
57. J. Laskar *et al.*, A long-term numerical solution for the insolation quantities of the Earth. *Astron. Astrophys.* **428**, 261–285 (2004).
58. L. N. Harrison *et al.*, Travertine records climate-induced transformations of the Yellowstone hydrothermal system from the late Pleistocene to the present. *Geol. Soc. Am. Bull.* **136**, 3605–3618 (2024).
59. V. Iglesias, T. R. Krause, C. Whitlock, Complex response of white pines to past environmental variability increases understanding of future vulnerability. *PLoS ONE* **10**, e0124439 (2015).
60. B. Shuman *et al.*, Holocene lake-level trends in the Rocky Mountains, United States. *Quat. Sci. Rev.* **28**, 1861–1879 (2009).
61. C. Whitlock *et al.*, Long-term relations among fire, fuel, and climate in the north-western US based on lake-sediment studies. *Int. J. Wildland Fire* **17**, 72–83 (2008).
62. B. N. Shuman, M. Serravezza, Patterns of hydroclimatic change in the Rocky Mountains and surrounding regions since the last glacial maximum. *Quat. Sci. Rev.* **173**, 58–77 (2017).
63. N. J. Chellman *et al.*, High elevation ice patch documents Holocene climate variability in the northern Rocky Mountains. *Quat. Sci. Adv.* **3**, 100021 (2021).
64. Y. Zhuang, R. Fu, B. D. Santer, R. E. Dickinson, A. Hall, Quantifying contributions of natural variability and anthropogenic forcings on increased fire weather risk over the western United States. *Proc. Natl. Acad. Sci. U.S.A.* **118**, e2111875118 (2021).
65. A. L. Westerling, Increasing western US forest wildfire activity: Sensitivity to changes in the timing of spring. *Philos. Trans. R. Soc. Lond. B, Biol. Sci.* **371**, 20150178 (2016).
66. D. J. Larsen, S. E. Crump, A. Blumm, Alpine glacier resilience and neoglacial fluctuations linked to Holocene snowfall trends in the western United States. *Sci. Adv.* **6**, eabc7661 (2020).
67. G. T. Pederson *et al.*, Dynamic treeline and cryosphere response to pronounced mid-Holocene climatic variability in the US Rocky Mountains. *Proc. Natl. Acad. Sci. U.S.A.* **122**, e2412162121 (2025).
68. S. Hostetler *et al.*, *Greater Yellowstone Climate Assessment: Past, Present, and Future Climate Change in Greater Yellowstone Watersheds* (Montana State University, Institute on Ecosystems, 2021), p. 258.
69. M. G. Turner, K. H. Braziunas, W. D. Hansen, B. J. Harvey, Short-interval severe fire erodes the resilience of subalpine lodgepole pine forests. *Proc. Natl. Acad. Sci. U.S.A.* **116**, 11319–11328 (2019).
70. H. E. Wright, D. H. Mann, P. H. Glaser, Piston corers for peat and lake sediments. *Ecology* **65**, 657–659 (1984).
71. K. D. Bennett, K. J. Willis, "Pollen" in *Tracking Environmental Change Using Lake Sediments*, J. P. Smol, H. J. B. Birks, W. M. Last, R. S. Bradley, K. Alverson, Eds. (Kluwer Academic Publishers, 2001), pp. 5–32.
72. R. O. Kapp, O. K. Davis, J. E. King, O. Ronald, *Kapp's Pollen and Spores* (American Association of Stratigraphic Palynologists, ed. 2, 2000). p. 279.
73. P. E. Higuera, D. G. Gavin, P. J. Bartlein, D. J. Hallett, Peak detection in sediment–charcoal records: Impacts of alternative data analysis methods on fire-history interpretations. *Int. J. Wildland Fire* **19**, 996–1014 (2011).
74. R. W. Battarbee, V. J. Jones, R. J. Flower, N. G. Cameron, "Diatoms" in *Tracking Environmental Change Using Lake Sediments*, J. P. Smol, H. J. B. Birks, W. M. Last, R. S. Bradley, K. Alverson, Eds. (Kluwer Academic Publishers, 2001), pp. 155–202.
75. L. Bahls, Ed., "Northwest diatoms: a photographic catalogue of species in the Montana Diatom Collection, with ecological optima, associates, and distribution records for the nine northwestern Unived States" in *Northwest Diatoms* (The Montana Diatom Collection, Helena, MT, 2005), vol. 2, p. 464.
76. S. A. Spaulding *et al.*, Diatoms of North America. *Diatom Res.* **36**, 291–304 (2021).
77. J. R. Alder, S. W. Hostetler, Global climate simulations at 3,000 year intervals for the last 21,000 years with the GENMOM coupled atmosphere–ocean model. *Clim. Past* **10**, 2925–2978 (2014).
78. J. R. Alder, S. W. Hostetler, Dynamical downscaling of the GENMOM climate model over western North America from the Last Glacial Maximum to present. *Data.gov*. https://doi.org/10.5066/P1M74HJI. Accessed 27 July 2026.
79. R. E. Dickinson, A. Henderson-Sellers, P. J. Kennedy, "Biosphere atmosphere transfer scheme (BATS) version le as coupled to the NCAR community climate model" (NCAR Technical Note NCAR/TN-387+STR, National Center for Atmospheric Research, 1993) p. 72. https://opensky.ucar.edu/system/files/2024-08/technotes_154.pdf. Accessed 27 July 2026.
80. N. Elguindi *et al.*, *Regional Climate Model RegCM Reference Manual Version 4.7* (The Abdus Salam International Centre for Theoretical Physics, 2017), p. 49.
81. C. M. Schiller, C. Whitlock, Feather Lake pollen dataset (Version 1.0) [Dataset]. Neotoma Paleoecology Database. https://doi.org/10.21233/4EC8-Y804. Accessed 26 July 2026.
82. C. M. Schiller, Feather Lake X-ray fluorescence (XRF) dataset (Version 1.0) [Dataset]. Neotoma Paleoecology Database. https://doi.org/10.21233/0X5T-5B68. Accessed 26 July 2026.
83. C. M. Schiller, Lower Basin Lake X-ray fluorescence (XRF) dataset (Version 1.0) [Dataset]. Neotoma Paleoecology Database. https://doi.org/10.21233/GYYK-GJ98. Accessed 26 July 2026.
84. C. M. Schiller, East Twin Buttes lake X-ray fluorescence (XRF) dataset (Version 1.0) [Dataset]. Neotoma Paleoecology Database. https://doi.org/10.21233/W5NH-MS53. Accessed 26 July 2026.
85. C. M. Schiller, Rush Lake X-ray fluorescence (XRF) dataset (Version 1.0) [Dataset]. Neotoma Paleoecology Database. https://doi.org/10.21233/Q3BV-VQ46. Accessed 26 July 2026.
86. C. M. Schiller, C. Whitlock, Rush Lake pollen dataset (Version 1.0) [Dataset]. Neotoma Paleoecology Database. https://doi.org/10.21233/qa1b-nk38. Accessed 26 July 2026.
87. C. M. Schiller, Rush Lake X-ray fluorescence (XRF) dataset (Version 1.0) [Dataset]. Neotoma Paleoecology Database. https://doi.org/10.21233/J7TT-MF60. Accessed 26 July 2026.
88. C. M. Schiller, Rush Lake X-ray fluorescence (XRF) dataset (Version 1.0) [Dataset]. Neotoma Paleoecology Database. https://doi.org/10.21233/BEPS-HF29. Accessed 26 July 2026.
89. S. R. Brown, Rush Lake diatom dataset (Version 1.0) [Dataset]. Neotoma Paleoecology Database. https://doi.org/10.21233/HN5Z-R429. Accessed 26 July 2026.